Linking glacial-interglacial states to multiple equilibria of climate

www.reading.ac.uk/centaur

CentAUR

Central Archive at the University of Reading

Linking Glacial-Interglacial States to Multiple Equilibria of Climate

David Ferreira[1] [ID] **, John Marshall[2], Takamitsu Ito[3]** [ID] **, and David McGee[2]** [ID]

[1]Department of Meteorology, University of Reading, Reading, UK, [2]Department of Earth, Atmospheric and Planetary Sciences, Massachusetts Institute of Technology, Cambridge, MA, USA, [3]School of Earth and Atmospheric Sciences, Georgia Institute of Technology, Atlanta, GA, USA

Key Points:
- Multiple equilibria of the global climate are found in a coupled ocean-atmosphere-sea ice general circulation model
- The two equilibrium states exhibit similarities with the present day climate and that of the Last Glacial Maximum
- The amplitude of the glacial-interglacial cycles may be set by such equilibrium states, rather than by the forcing and feedbacks

Supporting Information:
- Supporting Information S1
- Figure S1
- Figure S2
- Figure S3
- Figure S4
- Figure S5
- Figure S6

Abstract Glacial-interglacial cycles are often described as an amplified global response of the climate to perturbations in solar radiation caused by oscillations of Earth's orbit. However, it remains unclear whether internal feedbacks are large enough to account for the radically different glacial and interglacial states. Here we provide support for an alternative view: Glacial-interglacial states are multiple equilibria of the climate system that exist for the same external forcing. We show that such multiple equilibria resembling glacial and interglacial states can be found in a complex coupled general circulation model of the ocean-atmosphere-sea ice system. The multiple states are sustained by ice-albedo feedback modified by ocean heat transport and are not caused by the bistability of the ocean's overturning circulation. In addition, expansion/contraction of the Southern Hemisphere ice pack over regions of upwelling, regulating outgassing of CO_2 to the atmosphere, is the primary mechanism behind a large pCO_2 change between states.

Plain Language Summary For the last three million years, Earth's climate has oscillated between interglacial states (like today's climate) and glacial states (when ice sheets covered North America and Scandinavia). The dynamics of these glacial-interglacial cycles (GICs) remains elusive. Here we provide evidence that GICs may be supported by multiple equilibrium of Earth's climate. In a coupled climate model with idealized geometry, we reveal two equilibrium states that coexist for the same external forcing. These states, which are sustained by ice-albedo feedback modified by ocean heat transport, resemble the glacial and interglacial states. If confirmed, a link between GICs and multiple stable states would have a profound impact on our interpretation of the paleo-record, and notably on the relationship between changes in the insolation due to Earth's orbital cycles and GICs. This link may provide an answer to puzzling aspects of the GIC, for example, why their amplitude is so regular despite the highly variable magnitude of insolation change during glacial terminations. In our perspective, the GIC's amplitude is primarily set by the separation between the multiple states (an intrinsic property of the unperturbed system) rather than by the forcing. The latter then provides the kick to trigger the transition from one state to the other.

1. Introduction

Over the last three million years, Earth's climate has flipped between warm/interglacial conditions, such as the present-day Holocene, and cold/glacial conditions, similar to those found at the Last Glacial Maximum (LGM) 21 kyr ago (Petit, 1999; Raymo et al., 2006). The glacial-interglacial cycles (GICs) have been linked to variations of Earth's orbital parameters (Milankovitch cycles), namely, precession, obliquity, and eccentricity, which vary, respectively, with dominant periods of roughly 20, 40, and 100 kyr. However, evidence supporting a link between GIC and Milankovitch cycles is foremost statistical (Hays et al., 1976; Huybers, 2011; Raymo et al., 2006). There is no generally accepted mechanism by which the Milankovitch cycles drive the GIC (Paillard, 2015).

A puzzling aspect of the astronomical hypothesis is that small global insolation fluctuations must drive large global shifts of the climate system. This is typically addressed by invoking either strong internal feedbacks or some nonlinear mechanism. If strong internal feedbacks are at play, land/sea ice-albedo feedbacks (combined with large local insolation changes) and CO_2 feedbacks are most likely. This behavior has been encapsulated in conceptual models (Imbrie & Imbrie, 1980; Parrenin & Paillard, 2003), but it remains unclear whether the feedbacks in more realistic models would be large enough to achieve the observed climate shifts in response

to the solar forcings. As yet there is no example of a GCM simulating GICs when solely forced with Milankovitch cycles, in the absence of prescribed feedbacks such as land-ice and CO_2 changes.

Taking a nonlinear perspective, various studies have explored the possibility of free oscillations of the climate system, paced or phased-locked by the Milankovitch forcing (Gildor & Tziperman, 2000; Le Treut & Ghil, 1983; Saltzman et al., 1984). Others hypothesized that glacial and interglacial states are two possible equilibrium states of Earth's climate (Benzi et al., 1982; Nicolis, 1982; Paillard, 1998). In this case, the Milankovitch radiative forcing provides the "kicks" necessary for the climate system to exceed thresholds and transition between states.

However promising, the latter perspective of the GIC builds on the major assumption that the climate system possesses multiple equilibrium states for a given external forcing. This behavior is commonly found in low-order or conceptual models such as the Budyko-Sellers energy balance model, which possess multiple equilibria through sea-ice albedo feedback (North et al., 1981; Rose & Marshall, 2009). However, it is unclear whether more complex systems, and ultimately Earth's climate, can sustain global multiple equilibrium states which resemble glacial and interglacial states.

Here, building on previous developments (Ferreira et al., 2011), we first demonstrate that multiple stable states can be sustained in a complex fully dynamical ocean-atmosphere-sea ice general circulation model configured with an idealized Earth-like geometry. Second, we show that these equilibrium states exhibit striking similarities to our present-day climate and the climate of the LGM, including signatures of biogeochemical cycles.

2. Modeling Context

Simulations are carried out with the MIT GCM (Marshall et al., 1997), which solves for the three-dimensional circulation of atmosphere and ocean, and includes sea ice and land surface processes. The atmospheric physics is of "intermediate" complexity, based on the Simplified Parametrizations, primitivE-Equation DYnamics (Molteni, 2003) at low vertical resolution (further details in the supporting information Text S1). The configuration (Figure 1) comprises two 45°-wide land masses defining a narrow Atlantic-like basin and a wide Pacific-like basin connecting to an unblocked Southern Ocean (SO). This simplified geometry includes many of the essential dynamics that shape Earth's climate system (e.g., hydrological cycle, storm tracks). It also captures two key asymmetries: an asymmetry between the two northern basins with the absence of deep water formation in the Pacific (Ferreira et al., 2018) and a north-south asymmetry between a northern wind-driven gyre regime and a vigorous SO circumpolar current.

In GIC theories, atmospheric CO_2 changes can be described as a primary driver, a key feedback or an amplifier that can be ignored (see, e.g., Paillard, 2015). Our primary goal here is to demonstrate, in an Earth-like geometry, the possibility of multiple equilibria driven by the dynamical components of the climate system. We focus on the "fast" ocean-atmosphere-sea ice components, neglecting potential feedbacks from, notably, land ice and CO_2. To facilitate comparison of our results with observations, we also compute the "fingerprints" of the dynamically driven multiple states on a *passive* carbon cycle model (i.e., one in which CO_2 does not feedback through radiation on the climate state).

Two stable equilibria of climate are supported, one "Cold" and one "Warm" for the same external forcing and parameters, thus demonstrating that multiple equilibria are possible in a coupled GCM comprising a myriad of degrees of freedom. The difference in the climate of the two states is of planetary scale. Global average sea surface temperature and surface air temperature differ by 8.2 and 13.5 °C, respectively (patterns are shown in Figure S1). In the southern hemisphere (SH), the sea ice edge (as measured by the 15% annual mean concentration) expands by about 15° of latitude in the Cold state (Figure 1). The northern hemisphere, which is nearly ice free in the Warm state, exhibits a large ice cap extending over the subpolar gyre (45°N) in the Cold state, with a similar expansion of snow cover over land (Figure 1, top left).

Previous studies of the aquaplanet (Ferreira et al., 2011; Rose, 2015; Rose & Marshall, 2009; Rose et al., 2013) have revealed that multiple states of the kind shown in Figure 1 owe their existence to a fundamental and robust feature of the ocean circulation: the ocean heat transport (OHT) peaks near 15–20°N/S and drops sharply in the midlatitudes (Figure 2, top right). This reflects the presence on both sides of the equator of shallow (0–400 m) wind-driven overturning cells associated with the trade winds (Figure 2), which transport
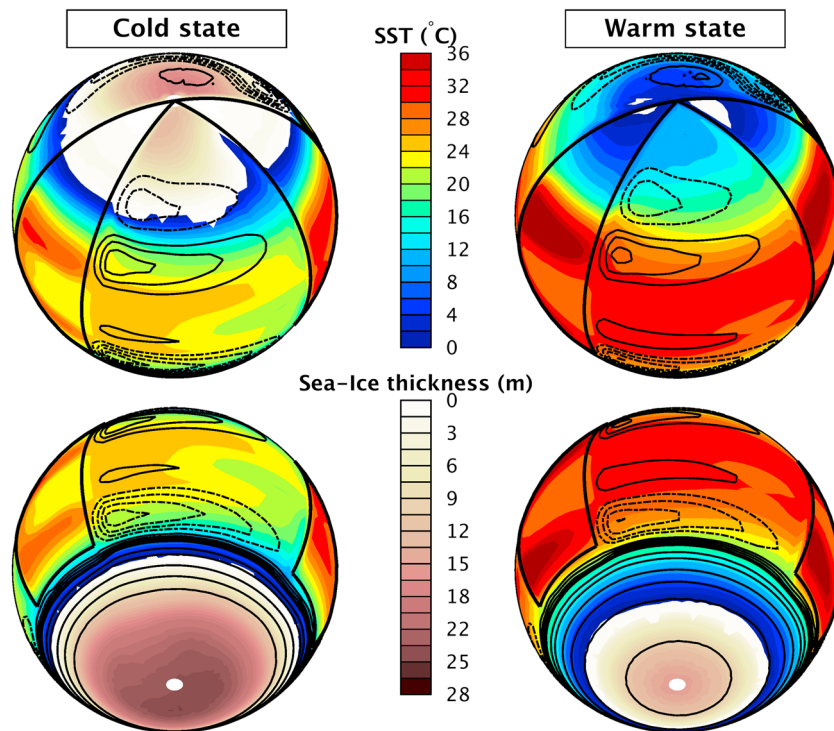
Figure 1. Temperature and ice distributions in the two equilibrium states. Sea Surface Temperature (blue-red shading, in ° C) and sea ice thickness (white-brown shading, in meter) for the (left) Cold and (right) Warm states. Over the continents, the Surface Air Temperature and snow depth are shown instead. The thick solid line denotes the continental boundaries. The barotropic streamfunction for the ocean is shown in black contours (solid for clockwise, dashed for counter clockwise). Both states are obtained for the same external forcing and same parameters.

warm surface waters from the equator into middle latitudes. The pronounced OHT convergence in the subtropics can arrest a runaway expansion of sea ice through the ice-albedo feedback and permits the existence of a steady state with a large ice cap encroaching down into midlatitudes. Another equilibrium state is possible with nearly ice-free conditions, in which ice albedo feedback promoting the sea ice expansion is weak and easily balanced by the ocean and atmosphere heat transport to the poles. The large ice cap state is unstable in the classic Budyko-Sellers model but stabilized in our GCM by the structure of OHT. This is formalized in a modified Budyko-Sellers-type model (Ferreira et al., 2011; Rose & Marshall, 2009) which predicts a stable ice edge on the poleward side of the peak OHT, consistent with our GCM simulations (Figure 2, top right and Figure S2).

Previous thinking about the role of multiple equilibria in past climate changes has been dominated by the idea that the Atlantic meridional overturning circulation (AMOC) possesses bistability with an "on" and an "off" state. Abrupt switching between the "on" and "off" modes (triggered by freshwater perturbations) is often invoked to interpret events such as Dansgaard-Oeschger events (Alley et al., 2003, but see Wunsch, 2007, and Seager & Battisti, 2007, for a critical evaluation). Paleoproxies provide little evidence for a full AMOC collapse at the LGM and rather suggest that a weaker and shallower cell remained active (Burckel et al., 2016; Gebbie, 2014; Lynch-Stieglitz et al., 2007). The AMOC bistability is primarily an oceanic process (Stommel, 1961). Signatures of an AMOC collapse are concentrated in the North Atlantic basin with relatively weak (and model dependent) signals outside the Atlantic sector (Manabe & Stouffer, 1988; Mecking et al., 2016; Vellinga & Wood, 2002). The multiple states described here differ fundamentally from AMOC bistability and are supported by coupled ocean-atmosphere-sea ice dynamics. Although the MOC does change between states in our simulations (Figure 3), this change does not correspond to a collapse and is in fact a symptom rather than a driver of the bistability (Ferreira et al., 2011). Moreover, the equilibrium states are associated with climate shifts of global extent (Figure 1) comparable to those observed in the past, providing a novel framework to interpret past climate changes.
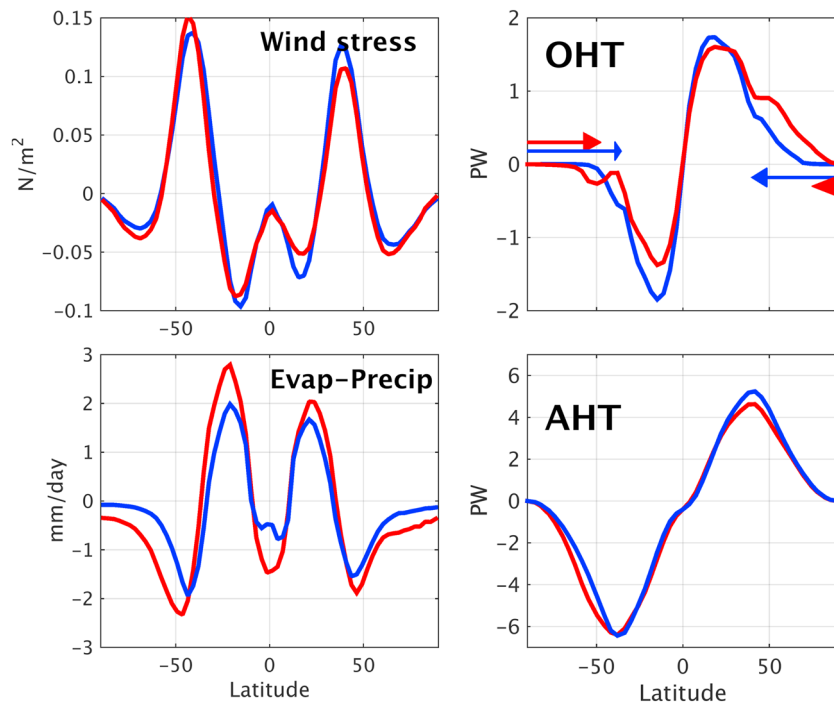
Figure 2. Surface zonal wind stress (N/m², top left), evaporation minus precipitation (mm/day, bottom left) and the net energy transports (in PW $=10^{15}$ W) in the ocean (top right) and atmosphere (bottom, right). The Warm and Cold states are denoted by red and blue lines, respectively. Horizontal arrows indicate the sea ice extent (15% sea ice fraction) where the length of the arrowheads denote the minimum/maximum seasonal range.

3. Circulation Patterns in Warm and Cold States

As expected, the Cold state exhibits a weaker hydrological cycle than the Warm state, as illustrated by the smaller amplitude of the evaporation minus precipitation field (Figure 2), consistent with the "dry gets drier and wet gets wetter" principle seen in global warming experiments (Held & Soden, 2006). The SH jet stream weakens slightly (by ~10%) and shifts northward (by 1.5° lat) in the Cold state, reflecting a northward displacement of the baroclinic zone (strong surface temperature gradient) following the sea ice expansion (further details on the atmospheric states in Text S2 and Figure S3).

Differences between equilibrium states are also pronounced in the deep ocean. The Cold state has an intensified bottom cell (10 Sv cf. 3 Sv of Warm state) emanating from the south (Figure 3, left). These waters, analogous to Antarctic Bottom Water (AABW) of the present-day ocean, are produced by brine rejection in the regions of production and export of sea ice. As the southern source is stronger in the Cold state, bottom waters approach the freezing point everywhere (~ −1.5 °C from 7 °C in the Warm state) and become saltier by ~0.5 psu. In contrast, the upper overturning cell (above ~2,000 m) is weaker in the Cold state by 5 Sv (Figure 3). This is not the result of a change in the SH westerly winds and associated upwelling rates. Rather, it is the consequence of a shift in the partitioning of upwelled water between the upper and lower cells: While upwelling mainly feeds the upper cell in the Warm state, upwelled waters are equally partitioned between the upper and lower cells in the Cold state.

The reorganization of the global overturning is consistent with conceptual models highlighting the role of the SH surface buoyancy fluxes in controlling the global MOC, and the depth of the interface between the upper and lower overturning cells (Burke et al., 2015; Ferrari et al., 2014; Marzocchi & Jansen, 2017; Sun et al., 2018; Watson et al., 2015). In steady state, poleward (equatorward) flowing surface waters must lose (gain) buoyancy to (from) the atmosphere and sea ice (Marshall, 1997; Marshall & Radko, 2003). Within the ice pack, the ocean experiences net buoyancy loss as freezing and brine rejection dominate exchanges. A transition to net buoyancy gain occurs in the seasonal ice zone, where melting due to exported sea ice dominates. As the sea ice advances in the Cold state, the region of buoyancy loss expands northward (from 70 to 50° S) into the region of wind-driven upwelling, drawing a larger fraction of the upwelled water into the lower cell
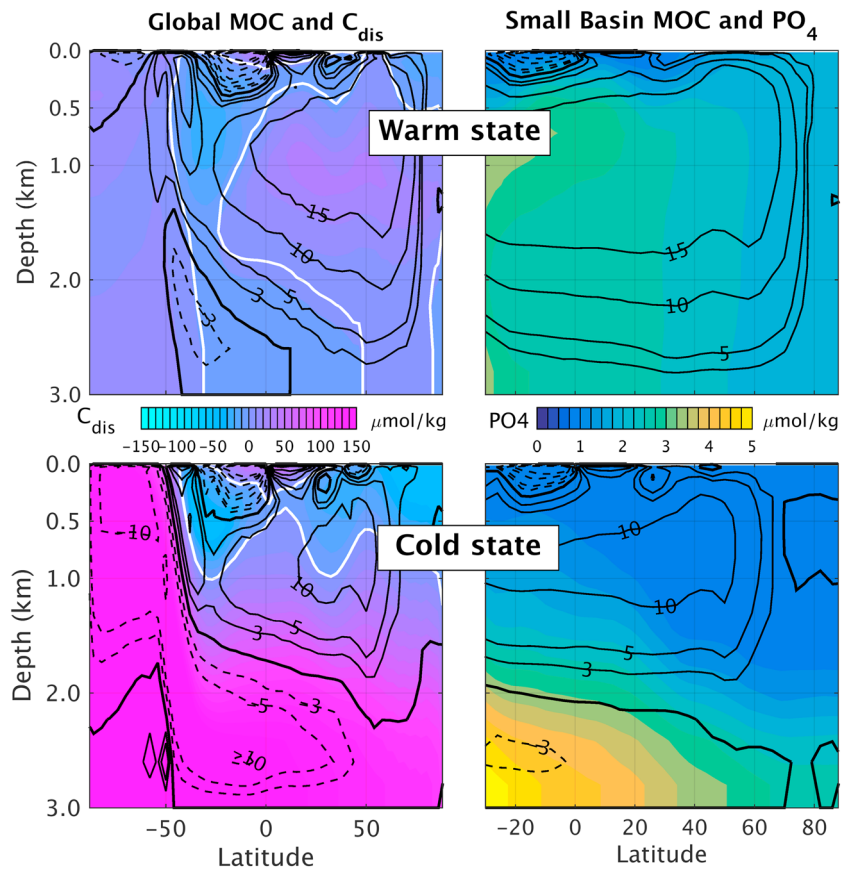
Figure 3. (Left) Global overturning circulation (in Sv, black lines) overlaid on the global disequilibrium reservoir C_{dis} (shading, in µmol/kg; zero contour highlighted with a thick white line). (Right) small basin overturning circulation overlaid on phosphate concentration (in µmol kg^{-1}). For the overturning, solid and dashed lines denote clockwise and counter-clockwise circulations, respectively. The Warm state is shown in the top row and the Cold state in the bottom row.

(Figure S4). In the adiabatic limit (Ferrari et al., 2014; Nikurashin & Vallis, 2012), this sea ice expansion also results in a shoaling of the interface between the two cells, as seen in our simulations (Figures 3 and S4). In a more realistic GCM including topographically driven mixing, deep water formation and buoyancy fluxes in the northern hemisphere may explain about half of the AMOC shoaling (Sun et al., 2018).

In the small (Atlantic-like) basin (Figure 3, right), the Cold state is associated with a weaker (but nonzero) upper cell (from 20 to 12 Sv), a shoaling of the dense water return flow, a southward shift of deep convection following the ice margin, and a stronger bottom cell fed from the south (see Figure S5 for the large basin overturning). The large increase in sea ice cover seals off the polar ocean and strongly suppresses air-sea buoyancy flux (see Figure S4).

Reorganization of the deep circulation between the two states has a profound impact on the distribution of tracers, as illustrated by the phosphate distribution (Figure 3, right). The nutrient load is dramatically enhanced in the deep ocean of the Cold state relative to the Warm state. While nutrient-depleted waters are only found in the top 300 m in the Warm state, they extend to 2,000 m in the Cold state where nutrients accumulate in the bottom cell and remain confined below 2,000 m outside of the SO.

4. Atmospheric pCO$_2$ and Biogeochemistry

A fascinating characteristic of the two equilibria is that the atmospheric CO$_2$ content is significantly lower in the Cold state (157 ppm) than in the Warm state (268 ppm). Both climate states contain the same carbon, phosphate and alkalinity inventories: the atmospheric CO$_2$ variation is an emergent property of the climate-carbon system resulting from the multiple equilibrium states (but recall that the CO$_2$ does not feed back on the radiative balance of the atmosphere).

A decomposition of the oceanic carbon reservoir (Ito & Follows, 2013) is used to diagnose the relative roles of different carbon pumps in the increased ocean carbon storage in the Cold state (see Text S3 for details). This increase is primarily driven by an increased air-sea disequilibrium pump C_{dis} (which measures the ocean carbon storage resulting from an imperfect equilibration between surface waters and the atmospheric pCO_2). This effect is reinforced by an increased solubility pump (due to the cooling between the Warm and Cold states) and is partially compensated by the weakened carbon storage associated with the biological pump (see Table S1 for a summary of the contributions).

In the Warm state, C_{dis} is near neutral (a global mean of +4.3 µmol/kg) consistent with the modern climatology (Figure 3, left), where the upper cell is weakly undersaturated ($C_{dis} < 0$) and the lower cell weakly supersaturated ($C_{dis} > 0$). In the Cold state, C_{dis} takes large positive values, indicating a strong supersaturation, equivalent to an atmospheric CO_2 drawdown of −87 ppm (Table S1). The increased C_{dis} is primarily found in the densest water masses confined to the bottom overturning cell (Figure 3, bottom left). These AABW-like water masses outcrop only in sea-ice covered regions of the SH, which strongly limits the outgassing of CO_2 to the atmosphere. The absence of equilibration between the surface waters and the atmosphere, before the latter are reinjected in the ocean interior, leads to the buildup of a large carbon reservoir within the bottom cell. To confirm this interpretation, we carry out a sensitivity experiment in which the capping effect of sea ice on air-sea CO_2 fluxes is removed at latitudes equatorward of the Warm state mean sea ice edge (in the SH only). As a result, the atmospheric CO_2 re-equilibrates at 210 ppm (from 157 ppm) after 4,600 years, directly attributing 53 ppm of pCO_2 change to the capping effect of the SH sea ice change between states. The remaining 34 ppm could be due to northern hemisphere sea ice effects and changes in residence time of waters at the surface. Note that, if anything, temperature effects would contribute a decrease, not an increase, of C_{dis}—see discussions in Toggweiler et al. (2003), Ito and Follows (2005), and Ödalen et al. (2018).

The glacial storage of CO_2 in the deep ocean by an expansion of the SH sea ice over the upwelling zone was first postulated by Stephens and Keeling (2000) using a simple box model in which sea ice cover is prescribed. This idea has been challenged arguing that the seasonal cycle of sea ice cover can expose a significant fraction of the upwelling regions to air-sea equilibration through melting and opening of the sea ice (Morales Maqueda & Rahmstorf, 2002; Sun & Matsumoto, 2010). Our calculation explicitly represents the seasonal cycle of sea ice cover and its impact on the air-sea gas transfer, as well as its impact on primary production through the availability of light (Kurahashi-Nakamura et al., 2007). The generation of leads by sea ice dynamics, however, is absent here, although its net effect on CO_2 storage is unclear (as the presence of leads increase air-sea carbon exchanges as well as primary production). Nonetheless, the modeled Warm state successfully reproduces the observed distribution of modern C_{dis} (Ito & Follows, 2013). Our simulations thus lend strong support for such a mechanism provided that the sea ice expansion reaches into the SO upwelling region. It is likely that the reorganization of the MOC also contributes significantly, as a larger fraction of the upwelled water in the SO is transported southward under the Cold state.

It should be noted that our model overestimates the solubility-driven CO_2 drawdown (−58 ppm) because of the large decline in the mean ocean temperature (−7.7 °C). For a realistic ocean cooling (2–4 °C), we estimate it would be −23 ± 8 ppm, reducing the total CO_2 drawdown to −71± 7 ppm (Table S1).

The biological carbon storage is reduced in the Cold state, primarily due to the reorganization of the deep circulation and the dominance of AABW-like water with an elevated preformed phosphorus. In contrast, the surface phosphate is strongly depleted in the ice-free regions of the SH, leading to the decline in the phosphate inventory of the upper overturning cell. The sea ice expansion in the Cold state weakens the biological productivity in the southern high latitudes, consistent with paleo-productivity proxies (Jaccard et al., 2013; Kohfeld et al., 2005). Combining the effects of organic and carbonate pumps (see Text S3), the net biological pump increases the atmospheric CO_2 by +36 ppm. When connecting our results to the inferred changes from paleoproxies, the role of the biological carbon pump is the most notable limitation of our study. In particular, our model does not reproduce the elevated glacial productivity in the sub-Antarctic latitudes, perhaps due to the lack of iron cycling (Kohfeld et al., 2005). This weakened productivity causes an elevated level of deep water oxygen due to the reduced respiratory O_2 loss, which is inconsistent with bottom water O_2 reconstructions (Jaccard & Galbraith, 2011; Jaccard et al., 2009). The overestimation of ocean cooling also raises the solubility of oxygen, leading to an additional positive bias in the deep O_2 (further discussion of the carbon pumps is found in Text S4).
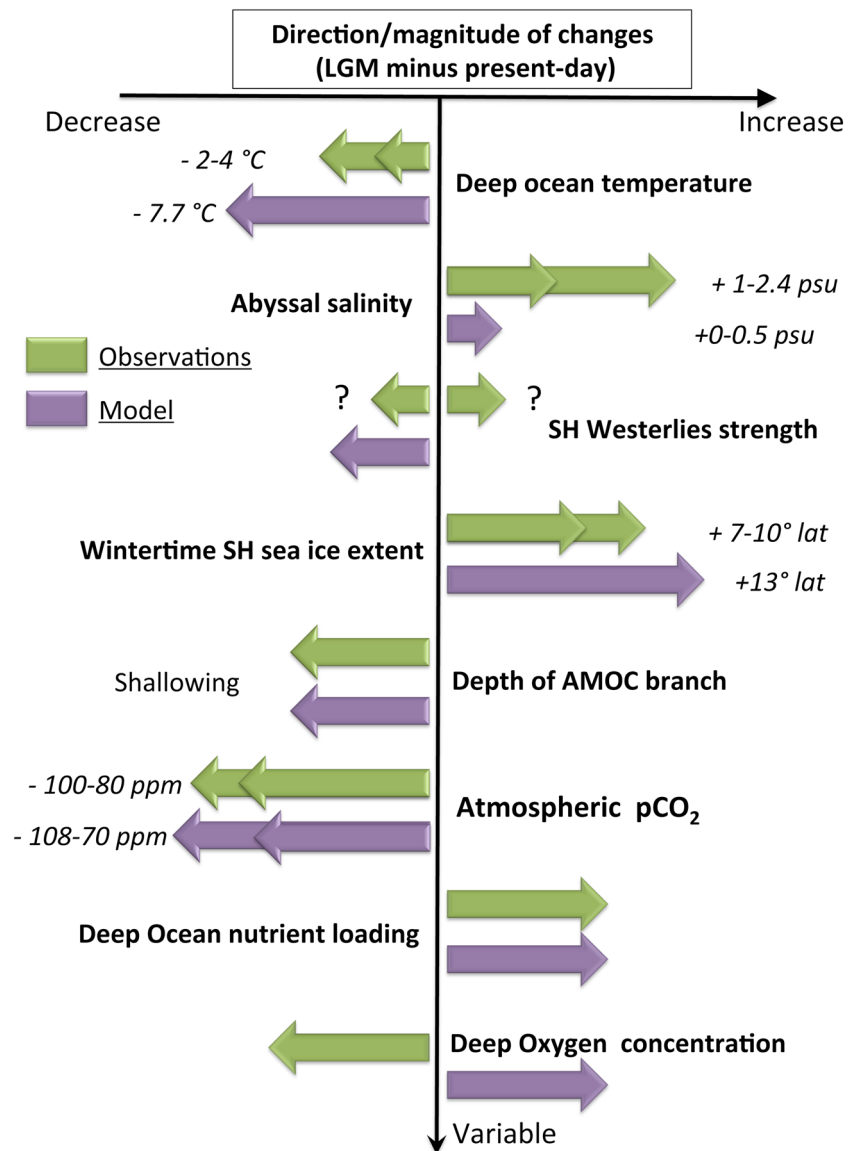
Figure 4. Observed changes between the Last Glacial Maximum and present-day climates from observations (green arrows) along with the corresponding differences between the Cold and Warm states of our idealized Earth-like climate simulations (purple arrows). When possible, arrows are scaled to represent the magnitude of the changes. Double arrows indicate the range of uncertainties.

Despite this limitation, our model reproduces several important features of glacial carbon cycling. Phosphate accumulates in the deep water and is depleted in the upper water column (Figure 3), consistent with nutrient proxies (Boyle, 1988; Jaccard et al., 2009). While Antarctic preformed nutrient concentrations are relatively high in our model, the deep water still contains a high level of DIC in the lower limb of the MOC due to the elevated level of C_{dis}. This allows the retention of excess DIC in the bottom water while avoiding the widespread anoxia that would occur if the carbon sequestration was dominated by C_{org}.

5. Comparing to the Observed Glacial and Interglacial States

Differences between our Warm and Cold states show striking similarities with interglacial and glacial states as inferred from the present climate and that of the LGM, respectively (Figure 4). Comparison to the present day and LGM is motivated by data availability, and does not imply that all glacial and interglacial states are identical (Past Interglacials Working Group of PAGES, 2016). However, variations among these peak states of the GIC is much smaller than the glacial-interglacial differences, which are the focus of our comparison.

Reconstruction of the SO sea ice edge for the LGM indicates a wintertime equatorward displacement between 7 and 10° of latitude relative to present time (Gersonde et al., 2005), which is of the same magnitude as our simulated ice expansion (13° of latitude). Estimates for the summertime LGM are more uncertain but suggest a patchy expansion with large values in the Weddell sector (up to 15° of latitude) and no change in the Indian sector (the sea ice retreating almost back to the coast as today). Our model cannot capture these asymmetries and is likely most relevant to the Weddell sector where the coast is much further south. There, the estimated (15°) and simulated (18°) summertime changes are similar.

Although the strength and position of the SH westerly winds in the glacial periods has received much attention as a possible driver of the atmospheric CO_2 change (Toggweiler, 2009), paleoproxy data are very uncertain (Kohfeld et al., 2013; Shulmeister et al., 2004) while simulations of the LGM show very little agreement among models (Sime et al., 2016). In our simulations, changes in the SH jet stream (Figure 2) have little impact on CO_2, which is mainly driven by changes in sea ice cover.

In the North Atlantic, paleoproxies suggest that the LGM wintertime sea ice cover was greatly expanded, covering the Nordic Seas and most of the subpolar gyre (de Vernal et al., 2005) and possibly down to the British Isles during stadial conditions (Dokken et al., 2013). Reconstructions also suggest a southwest-northeast tilted edge along the path of the North Atlantic drift, as seen in our model.

The large shift in deep ocean nutrients between the Warm and Cold states (Figure 3, left) is consistent with estimates for the present-day and LGM (Boyle & Keigwin, 1985). To help connect with available proxies (Curry & Oppo, 2005; Peterson et al., 2014), estimates of the equivalent $\delta^{13}C$ distributions for the two states are shown in Figure S6. Notwithstanding limitations due to the idealized geometry, the two states capture important large-scale changes seen in observations, notably the near doubling of the top-to-bottom $\delta^{13}C$ gradient at the LGM (Curry & Oppo, 2005; Peterson et al., 2014). These rearrangements of the tracer distributions (e.g., $\delta^{13}C$) have been interpreted as reflecting a slightly weaker and shallower AMOC at the LGM (Curry & Oppo, 2005; Lynch-Stieglitz et al., 2007; Peterson et al., 2014). Although such interpretations should be taken with caution (Gebbie, 2014), we do observe a consistent set of changes in circulation/tracer patterns that parallels those inferred for the LGM.

Bottom waters at the LGM are estimated to be near the freezing point at all latitudes and saltier than today by 1 and 2.4 psu (Adkins et al., 2002). Similar tendencies are seen in our simulations although bottom salinity only increases by +0.5 psu in the SO, decreasing to zero at the North pole. As our model does not allow large accumulation of freshwater over land (we do not have ice sheets), the modeled salinity shifts provides an estimate of the contribution of ocean circulation changes and increased brine rejection to the observed change.

It is apparent that the temperature difference between the two states is larger than inferred for the LGM-present difference. This is traceable to a warm bias in northern surface temperatures of the Warm state, which is communicated to the global ocean through deep water formation (at ~ 7 °C compared to ~ 3 °C for the present day). This could be due to our idealized land distribution that facilitates OHT toward high latitudes and/or the narrow width of the continent that limits the advection of cold dry air over the oceans.

6. Conclusions

We have shown that multiple equilibria of global scale are possible in a complex coupled GCM with an Earth-like geometry. The robust dynamics that enables such states (a large heat release from the ocean to the atmosphere in midlatitudes; Ferreira et al., 2011; Rose & Marshall, 2009) suggests that they could exist in Earth's climate. Important similarities (both in terms of circulation and biogeochemical signatures) between our two climate states and that of the LGM/present-day suggest that GICs could be sustained by the existence of multiple equilibria. If confirmed, this would have a profound impact on our interpretation of the paleo-record, notably of the relationship between the Milankovitch cycles and the observed response.

Importantly, such a link does not imply that all glacial and interglacial states should be identical. Internal noise in the climate system (e.g., millennial AMOC variability), changes in the internal feedbacks (e.g., land ice and CO_2) and changes in the Milankovitch cycles could perturb trajectories through the "potential wells" of the multiple states. In fact, a more pressing question is why the GIC's amplitude is so regular considering the highly variable magnitudes of insolation change during glacial terminations (Petit, 1999). Linking the GIC to multiple stables states can provide an answer as in such case the GIC's amplitude is primarily determined by the separation between the multiple states (a property of the unperturbed system) rather than by the

forcing. The latter then provides the "kicks" to trigger the transition from one potential well to the other. Paillard's conceptual model illustrates these properties (Paillard, 1998): When driven by Milankovitch cycles, the magnitude of the cycles is relatively stable (compared to the variability in the forcing) but also allows for differences in the peak value and duration of the interglacials (see his Figure 4).

Our main goal here has been to reveal the possibility of multiple states sustained by the dynamical components of the climate system, and to put forward a novel perspective on the dynamics of GIC. Although our study represents a large step forward from the conceptual/analytical models used previously (e.g., Benzi et al., 1982; Paillard, 1998), critical issues remain to be addressed to advance this view. Future work should test whether these states persist in the presence of improved physics, notably land ice and radiative CO_2 feedbacks. Ice sheet dynamics are often proposed as an essential element of GIC dynamics (Abe-Ouchi et al., 2013; Imbrie & Imbrie, 1980; Muglia & Schmittner, 2015; Paillard, 1998), possibly responsible for the asymmetry between the fast deglaciations and the slower inceptions. The absence of a radiative CO_2 feedback in our experiments is also a major limitation as such a positive feedback may destabilize the multiple states. A simple sensitivity experiment in which a radiative perturbation of about -3 Wm^2 (equivalent to a $\sim$100 ppm pCO$_2$ drop) is imposed in the Cold state shows that this state remains stable although it is driven farther apart from the Warm state (not shown). As pointed out above, the separation between the states (in, say, global temperature) is most likely influenced by the highly idealized continental geometry employed here. Further evaluation of the multiple states, notably their similarity with Glacial/Interglacial states, will require use of a more realistic geometry. This is also essential to permit closer a comparison with available proxies.

The ideas presented here need to be tested in more complex GCMs. We feel that the search for such equilibria in climate models has been neglected and should be more systematic, as was done for example for the bistability of the overturning circulation.

References

Abe-Ouchi, A., Saito, F., Kawamura, K., Raymo, M. E., Okuno, J., Takahashi, K., & Blatter, H. (2013). Insolation-driven 100,000-year glacial cycles and hysteresis of ice-sheet volume. *Nature*, *500*, 190–194.

Adkins, J. F., McIntyre, K., & Schrag, D. (2002). The salinity, temperature and δ^{18}O of the glacial deep ocean. *Science*, *298*, 1769–1773.

Alley, R., Marotzke, J., Nordhaus, W. D., Overpeck, J. T., Peteet, D. M., Pielke, R. A., Jr. et al. (2003). Abrupt climate change. *Science*, *299*(5615), 2005–2010.

Benzi, R., Parisi, G., Sutera, A., & Vulpiani, A. (1982). Stochastic resonance in climatic change. *Tellus*, *34*, 10–16.

Boyle, E. A. (1988). Vertical oceanic nutrient fractionation and glacial/interglacial CO_2 cycles. *Nature*, *331*, 55–56.

Boyle, E. A., & Keigwin, L. D. (1985). Comparison of atlantic and pacific paleochemical records for the last 215,000 years: Changes in deep ocean circulation and chemical inventories. *Earth and Planet Science Letters*, *76*, 135–150.

Burckel, P., Waelbroeck, C., Luo, Y., Roche, D. M., Pichat, S., Jaccard, S. L., et al. (2016). Changes in the geometry and strength of the atlantic meridional overturning circulation during the last glacial (20–50 ka). *Climate Past*, *12*, 2061–2075.

Burke, A., Stewart, A. L., Adkins, J. F., Ferrari, R., Jansen, M. F., & Thompson, A. F. (2015). The glacial mid-depth radiocarbon bulge and its implications for the overturning circulation. *Paleoceanography*, *30*, 1021–1039. https://doi.org/10.1002/2015PA002778

Curry, W. B., & Oppo, D. W. (2005). Glacial water mass geometry and the distribution of δ^{13}C of CO_2 in the western atlantic ocean. *Paleoceanography*, *20*, PA1017. https://doi.org/10.1029/2004PA001021

de Vernal, A., Eynaud, F., Henry, M., Hillaire-Marcel, C., Londeix, L., Mangin, S., et al. (2005). Reconstruction of sea-surface conditions at middle to high latitudes of the northern hemisphere during the Last Glacial Maximum (LGM) based on dinoflagellate cyst assemblages. *Quaternary Science Reviews*, *24*, 897–924.

Dokken, T., Nisancioglu, K. H., Li, C., & Battisti, D. (2013). Dansgaard-oeschger cycles: Interactions between ocean and sea ice intrinsic to the nordic seas. *Paleoceanography*, *28*, 491–502. https://doi.org/10.1002/palo.20042

Ferrari, R., Jansen, M. J., Adkins, J. F., Burke, A., Stewart, A. L., & Thompson, A. F. (2014). Antarctic sea ice control on ocean circulation in present and glacial climates. *Proceedings of the National Academy of Sciences*, *111*(24), 8753–8758.

Ferreira, D., Cessi, P., Coxall, H. K., de Boer, A., Dijkstra, H. A., Drijfhout, S. S., et al. (2018). Atlantic-pacific asymmetry in deep-water formation. *Annual Review of Earth and Planetary Sciences*, *46*, 327–352.

Ferreira, D., Marshall, J., & Rose, B. (2011). Climate determinism revisited: Multiple equilibria in a complex climate model. *Journal of Climate*, *24*, 992–1012.

Gebbie, G. (2014). How much did glacial north atlantic water shoal? *Paleoceanography*, *29*, 190–209. https://doi.org/10.1002/2013PA002557

Gersonde, R., Crosta, X., Abelmann, A., & Armand, L. (2005). Sea-surface temperature and sea ice distribution of the southern ocean at the epilog last glacial maximum—A circum-antarctic view based on siliceous microfossil records. *Quaternary Science Reviews*, *24*, 869–896.

Gildor, H., & Tziperman, E. (2000). Sea ice as the galical cycles's climate switch: Role of seasonal and orbital forcing. *Paleoceanography*, *15*, 605–615.

Hays, J. D., Imbrie, J., & Shackleton, N. J. (1976). Variations in the Earth's orbit: Pacemaker of the ice ages. *Science*, *194*(4270), 1121–1132.

Held, I., & Soden, B. J. (2006). Robust responses of the hydrological cycle to global warming. *Journal of Climate*, *19*, 5686–5699.

Huybers, P. (2011). Combined obliquity and precession pacing of late pleistocene deglaciations. *Nature*, *480*, 229–232.

Imbrie, J., & Imbrie, J. Z. (1980). Modeling the climatic response to orbital variations. *Science*, *207*(4434), 943–953.

Ito, T., & Follows, M. J. (2005). Preformed phosphate, soft tissue pump and atmospheric CO_2. *Journal of Marine Research*, *63*, 813–839.

Ito, T., & Follows, M. J. (2013). Air-sea disequilibrium of carbon dioxide enhances the biological carbon sequestration in the southern ocean. *Global Biogeochemical Cycles*, *27*, 1–10. https://doi.org/10.1002/2013GB004682

Jaccard, S. L., & Galbraith, E. D. (2011). Large climate-driven changes of oceanic oxygen concentrations during the last deglaciation. *Nature Geoscience*, *5*, 151–156.

Jaccard, S. L., Galbraith, E. D., Sigman, D. M., Haugh, G. H., Francois, R. F., Petersen, T. F., et al. (2009). Subarctic pacific evidence for a glacial deepening of the oceanic respired carbon pool. *Earth and Planet Science Letters*, *277*, 156–165.

Jaccard, S. L., Hayes, C. T., Martinez-Garcia, A., Hodell, D. A., Anderson, R. F., Sigman, D. M., & Haugh, G. H. (2013). Two modes of change in southern ocean productivity over the past million years. *Science*, *339*, 1419–1423.

Kohfeld, K. E., Graham, R. M., de Boer, A. M., Sime, L. C., Wolff, E. W., Le Quéré, C., & Bopp, L. (2013). Southern hemisphere westerly wind changes during the last glacial maximum: Paleo-data synthesis. *Quarternary Science Reviews*, *68*, 76–95.

Kohfeld, K. E., Le Quéré, C., Harrison, S. P., & Anderson, R. F. (2005). Role of marine biology in glacial-interglacial CO_2 cycles. *Science*, *308*, 74–78.

Kurahashi-Nakamura, T., Abe-Ouchi, A., Yamanaka, Y., & Misumi, K. (2007). Compound effects of antarctic sea ice on atmospheric pCO_2 change during glacial–interglacial cycle. *Geophysical Research Letters*, *34*, L20708. https://doi.org/10.1029/2007GL030898

Le Treut, H., & Ghil, M. (1983). Orbital forcing, climatic interactions, and glaciation cycles. *Journal of Geophysical Research*, *88*(C9), 5167–5190.

Lynch-Stieglitz, J., Adkins, J. F., Curry, W. B., Dokken, T., Hall, I. R., Herguera, J. C., et al. (2007). Atlantic meridional overturning circulation during the last glacial maximum. *Science*, *316*, 66–69.

Manabe, S., & Stouffer, R. J. (1988). Two stable equilibria of a coupled ocean-atmosphere model. *Journal of Climate*, *1*, 841–866.

Marshall, D. (1997). Subduction of water masses in an eddying ocean. *Journal of Marine Research*, *55*(2), 201–222.

Marshall, J., Adcroft, A., Hill, C., Perelman, L., & Heisey, C. (1997). A finite-volume, incompressible Navier Stokes model for studies of the ocean on parallel computers. *Journal of Geophysical Research*, *102*(C3), 5753–5766.

Marshall, J., & Radko, T. (2003). Residual mean solutions for the antarctic circumpolar current and its associated overturning circulation. *Journal of Physical Oceanography*, *33*, 2341–2354.

Marzocchi, A., & Jansen, M. F. (2017). Connecting antarctic sea ice to deep-ocean circulation in modern and glacial climate simulations. *Geophysical Research Letters*, *44*, 6286–6295. https://10.1002/2017GL073936

Mecking, J. V., Drijfhout, S. S., Jackson, L. C., & Graham, T. (2016). Stable AMOC off state in an eddypermitting coupled climate model. *Climate Dynamics*, *47*, 2455–2470.

Molteni, F. (2003). Atmospheric simulations using a GCM with simplified physical parametrizations. I: Model climatology and variability in multi-decadal experiments. *Climate Dynamics*, *64*, 175–191.

Morales Maqueda, M. A., & Rahmstorf, S. (2002). Did antarctic sea-ice expansion cause glacial CO_2 decline? *Geophysical Research Letters*, *29*(1), 1011.

Muglia, J., & Schmittner, A. (2015). Glacial atlantic over-turning increased by wind stress in climate models. *Geophysical Research Letters*, *42*, 9862–9869. https://10.1002/2015GL064583

Nicolis, C. (1982). Stochastic aspects of climatic transitions—Response to a periodic forcing. *Tellus*, *34*, 1–9.

Nikurashin, M., & Vallis, G. K. (2012). A theory of the interhemispheric meridional overturning circulation and associated stratification. *Journal of Physical Oceanography*, *42*(10), 1652–1667.

North, G. R., Cahalan, R. F., & Jr, J. A. C. (1981). Energy balance climate models. *Reviews of Geophysics and Space Physics*, *19*, 91–121.

Ödalen, M., Nycander, J., Oliver, K. I. C., Brodeau, L., & Ridgwell, A. (2018). The influence of the ocean circulation state on ocean carbon storage and CO_2 drawdown potential in an earth system model. *Biogeosciences*, *15*, 1367–1393. https://10.5194/bg-15-1367-2018

Paillard, D. (1998). The timing of pleistocene glaciations from a simple multiple-state climate model. *Nature*, *391*, 378–381.

Paillard, D. (2015). Quaternary glaciations: from observations to theories. *Quaternary Science Reviews*, *107*, 11–24.

Parrenin, F., & Paillard, D. (2003). Amplitude and phase of glacial cycles from a conceptual model. *Earth and Planet Science Letters*, *214*, 243–250.

Past Interglacials Working Group of PAGES (2016). Interglacials of the last 800,000 years. *Reviews of Geophysics*, *54*, 162–219. https://doi.org/10.1002/2015RG000482

Peterson, C. D., Lisiecki, L. E., & Stern, J. V. (2014). Deglacial whole-ocean $\delta^{13}C$ change estimated from 480 benthic foraminiferal records. *Paleoceanography*, *29*, 549–563. https://doi.org/10.1002/2013PA002552

Petit, J. R. (1999). Climate and atmospheric history of the past 420,000 years from the Vostok ice core, Antarctica. *Nature*, *399*, 429–436.

Raymo, M. E., Lisiecki, L. E., & Nisancioglu, K. H. (2006). Plio-pleistocene ice volume, Antarctic climate, and the global $\delta^{18}O$ record. *Science*, *313*, 492–495.

Rose, B. (2015). Stable "water- belt" climates controlled by tropical ocean heat transport: A nonlinear coupled climate mechanism of relevance to snowball earth. *Journal of Geophysical Research: Atmospheres*, *120*, 1404–1423. https://doi.org/10.1002/2014JD022659

Rose, B., Ferreira, D., & Marshall, J. (2013). The role of oceans and sea ice in abrupt transitions between multiple climate states. *Journal of Climate*, *26*, 2862–2879.

Rose, B. E., & Marshall, J. (2009). Ocean Heat Transport, sea ice and multiple climatic states: Insights from Energy Balance Models. *Journal of the Atmospheric Sciences*, *66*, 2828–2843.

Saltzman, B., Hansen, A. R., & Maasch, K. A. (1984). The late quaternary glaciations as the response of a three-component feedback system to the earth-orbital forcing. *Journal of the Atmospheric Sciences*, *41*(23), 3380–3389.

Seager, R., & Battisti, D. S. (2007). *The Global Circulation of the Atmosphere*, Challenges to Our Understanding of the General Circulation: Abrupt Climate Change. Princeton, United States: Princeton University Press.

Shulmeister, J., Goodwin, G., Renwick, J., Harle, K., Armand, L., McGlone, M. S., et al. (2004). The southern hemisphere westerlies in the australasian sector over the last glacial cycle: A synthesis. *Quaternary International*, *118*, 23–53.

Sime, L. C., Hodgson, D., Bracegirdle, T. J., Allen, C., Perren, B., Roberts, S., & de Boer, A. M. (2016). Sea ice led to poleward-shifted winds at the last glacial maximum: The influence of state dependency on CMIP5 and PMIP3 models. *Climate of the Past Discussions*, *12*, 2241–2253.

Stephens, B. B., & Keeling, R. F. (2000). The influence of antarctic sea ice on glacial-interglacial CO_2 variations. *Nature*, *404*, 171–174.

Stommel, H. (1961). Thermohaline convection with two stable regimes of flow. *Tellus*, *13*(2), 224–230.

Sun, S., Eisenman, I., & Stewart, A. (2018). Does southern ocean surface forcing shape the global ocean overturning circulation? *Geophysical Research Letters*, *45*, 2413–2423. https://doi.org/10.1002/2017GL076437

Sun, X., & Matsumoto, K. (2010). Effects of sea ice on atmospheric pCO_2: A revised view and implications for glacial and future climates. *Journal of Geophysical Research*, *115*, G02015. https://doi.org/10.1029/2009JG001023

Toggweiler, J. R. (2009). Shifting westerlies. *Science*, *323*, 1434–1435.

Toggweiler, J. R., Gnanadesikan, A., Carson, S., Murnane, R., & Sarmiento, J. L. (2003). Representation of the carbon cycle in box models and gcms: 1. solubility pump. *Global Biogeochemical Cycles*, *17*(1), 1026. https://doi.org/10.1029/2001GB001401

Vellinga, M., & Wood, R. (2002). Global climatic impacts of a collapse of the atlantic thermohaline circulation. *Climate Change*, *54*, 251–267.

Watson, A. J., Vallis, G. K., & Nikurashin, M. (2015). Southern ocean buoyancy forcing of ocean ventilation and glacial atmospheric CO_2. *Nature Geoscience*, *8*, 861–864.

Wunsch, C. (2007). *Ocean circulation: Mechanisms and impacts—Past and future changes of meridional overturning*, chap. The past and future ocean circulation from a contemporary perspective. Washington, DC: American Geophysical Union.